ENABLING RAY TRACING FOR 5G

Vladislav Ryzhov

Department of Multimedia Technologies and Telecommunications,
Moscow Institute of Physics and Technology, Moscow, Russia
Yadro Telecom, Saint Petersburg, Russia

ABSTRACT

RT (Ray Tracing) models are widely used in RAN for channel modelling. Another possible application in processing chain of base station with multiple purposes: positioning, channel estimation/prediction, radio resources scheduling and others. In this paper RT positioning technique is addressed for Urban Outdoor scenario. Proposed robust approach achieves several meters accuracy even in NLOS and multipath conditions. Developed RT tracking was used for multiuser (MU) precoder prediction and demonstrated significant capacity gain. Also, this paper discloses practical aspects for achieving high accuracy.

KEYWORDS

Positioning, Ray Tracing, UL-AoA, multiuser precoder, GPS measurement, channel prediction, channel reciprocity.

1. INTRODUCTION

Positioning is an old task for wireless communications. The roughest and low-complex methods include identification by Cell-ID and RSS (Received Signal Strength). With high synchronization requirements [1] GPS and TDoA (Time Difference of Arrival) measurements increase positioning accuracy up to dozens of meters. Nowadays, base stations are equipped with large antenna arrays (e.g., 32T32R) and the current trend is to split panels into several ones [2-3] or use the single panel with the increased number of elements. Under these assumptions, angular domain represents most accurate method for positioning [4]. At the same time the most of the classic algorithms suffer from multipath propagation, LOS blockage, and variable channel conditions. Another future concept is cooperative MIMO, which is expected to improve spectral efficiency and coverage mostly by increasing a number of degrees of freedom and channel diversity [5].

The Proposed RT (Ray Tracing) positioning approach exploits multipoint reception and angular spectrum estimation. It is robust to complex propagation conditions and partly benefits from large scattering and multipoint reception. Due to joint RT processing of distributed AoA measurements proposed method is the most suitable for C-RAN (Cloud Radio Access Network) architecture. Also, such an approach can be used for real-time CSI (Channel State Information) or digital precoder prediction or provide more information for dynamic scheduling for operators.

RT requires high-precision maps for accurate localization. In this paper, we omit issues related to accumulation data for accurate map reconstruction. With multiple of automotive sensors, satellite images, cameras, etc. this map can be found. Although our approach does not require additional distributed synchronization, it assumes only intra-panel synchronization and calibration for angular spectrum estimation. Problems related to imperfect calibration,

interference directions, and inaccurate maps are solved via probabilistic weighting and clustering. Anyway, the map inaccuracy and antenna calibration are discussed in this paper.

The contribution of this paper is that it complements an approach for precise and robust RT positioning presented in [6] with practical restrictions. Also, it demonstrates performance gain from the use of RT tracking for channel prediction.

2. SYSTEM MODEL

2.1. Channel Model

The Uplink channel is modeled via RT in a certain outdoor environments, obtained from parsed 3D OSM (Open Street Map) with typically located UEs (User Equipment) and RRUs (Remote Radio Units) from open-source maps with mobile operator towers and their frequency bands.

2.2. Layout

Cooperating RRUs (with 120^0 sector antenna) are placed to satisfy ISD ≈ 150 m, tilt ≈ 10^0, a height ≈ 15-25 m. UEs are evenly spaced in the street at height of 1.5 m. For simplicity, each UE is equipped with one antenna with a uniform pattern, while RRU has a (4x8) horizontal antenna array with a 3GPP antenna element radiation pattern [7].

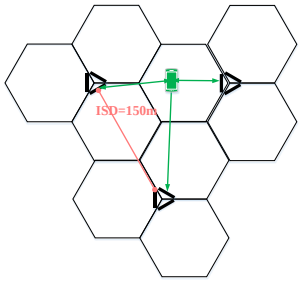

Figure 1. Layout with 3-sector antenna.

2.3. Signals

Each UE is configured [8] to send SRS (Sounding Reference Signal) in TDD mode with granularity K_TC = 2 and N_RB = 272 PRBs.

2.4. Overall Positioning Model

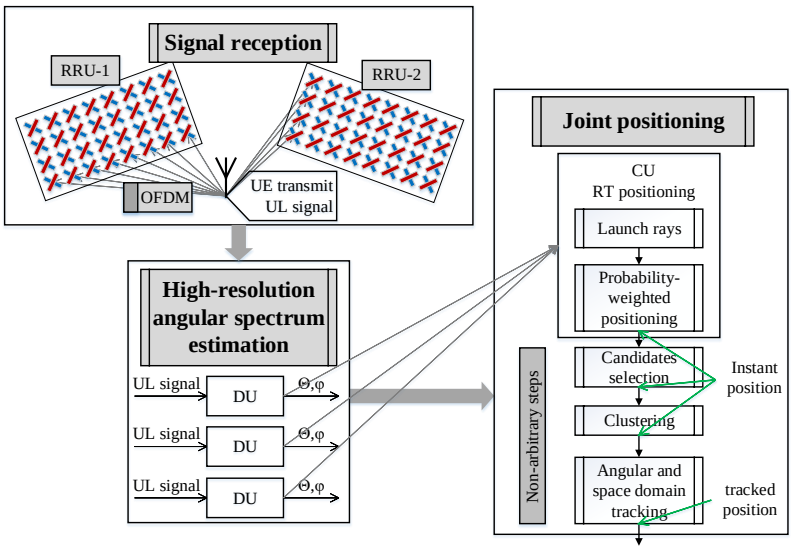

Figure 2. System model for positioning.

Multiple distributed RRUs cooperatively receive SRS, passed through the RT channel. After that, each DU (Distributed Unit) independently finds AoAs (Angles of Arrival) from the estimated angular spectrum. These estimates are reported to CU (Central Unit), which contains precise outdoor model. CU localizes UE from current instantaneous measurement via RT search in a direction of received angles. At this steps position represents a probabilistic estimate. Discarding and clustering of estimated positions is done to cope with outliers from imperfect angle estimation and map errors. Also, CU tracks measurements in the angular domain and expectation of positions for each cluster in the space domain in order to additionally discard false positions and smooth UE trajectory. To keep a trade-off between required accuracy and complexity we can exchange additional clustering or tracking complexity for higher accuracy.

3. RT CHANNEL MODEL

RT channel modeling has good accuracy [9] and papers [10-12] describe RT positioning. The developed C++ RT simulator has two main operating options: channel modeling and positioning. In both cases, it contains the following propagation patterns:

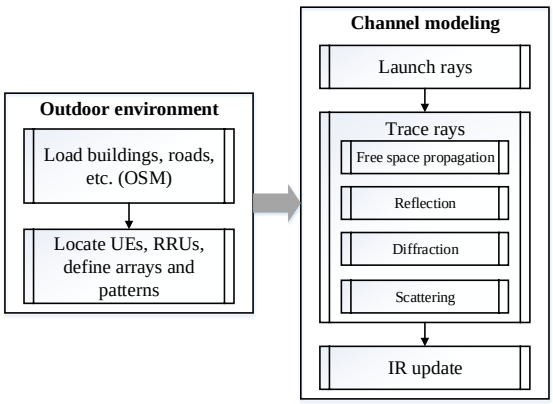

Figure 3. Concept of developed channel modelling via RT.

- Free space propagation

Solution of Helmholtz wave equation for point source in far field is a spherical wave, which defines phase and amplitude of propagating ray:

$$\mathbf{E}(\mathbf{r},\boldsymbol{\theta},\boldsymbol{\varphi}) = \frac{\mathbf{E_0}(\boldsymbol{\theta},\boldsymbol{\varphi})\mathbf{e}^{-\mathbf{ikr}}}{\mathbf{r}} \quad (1)$$

- Reflection

When interfered with by building, ground, etc. ray is reflected according to geometrical optics and reflection coefficients. From a Fresnel's equation reflection coefficients can be found from angles of incidence and reflection and electrical properties of material:

$$\mathbf{R}_{\perp} = \left|\frac{\boldsymbol{n_2}\cos(\boldsymbol{\theta_i}) - \boldsymbol{n_1}\cos(\boldsymbol{\theta_t})}{\boldsymbol{n_2}\cos(\boldsymbol{\theta_i}) + \boldsymbol{n_1}\cos(\boldsymbol{\theta_t})}\right|^2$$
$$\mathbf{R}_{||} = \left|\frac{\boldsymbol{n_2}\cos(\boldsymbol{\theta_t}) - \boldsymbol{n_1}\cos(\boldsymbol{\theta_i})}{\boldsymbol{n_2}\cos(\boldsymbol{\theta_t}) + \boldsymbol{n_1}\cos(\boldsymbol{\theta_i})}\right|^2 \quad (2)$$

- Scattering

Due to the roughness of surface, ray is scattered around the direction of reflection. Authors of [13] performed measurement campaign for scattering pattern of typical buildings and concluded that single-lobe directive model was the closest:

$$|\overline{\mathbf{E_S}}|^2 = \mathbf{E_{S0}^2}\left(\frac{\mathbf{1}+\cos\boldsymbol{\psi_R}}{\mathbf{2}}\right)^{\boldsymbol{\alpha_R}}, \boldsymbol{\alpha_R} = \mathbf{4} \quad (3)$$

- Diffraction

Paper [14] defines the most common Knife Edge Diffraction (KED) model:

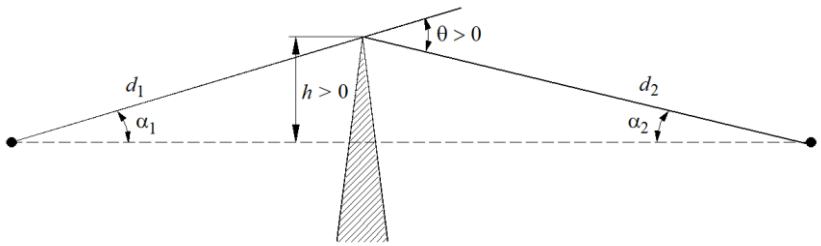

Figure 4. For definition v [14].

$$\mathbf{v} = \mathbf{h}\sqrt{\frac{\mathbf{2}}{\boldsymbol{\lambda}}\left(\frac{\mathbf{1}}{\mathbf{d_1}}+\frac{\mathbf{1}}{\mathbf{d_2}}\right)} \quad (4)$$

where electric field can be found from:

$$\mathbf{F}(\mathbf{v}) = \frac{\mathbf{E_{diffracted}}}{\mathbf{E_0}} = \frac{\mathbf{1}+\mathbf{i}}{\mathbf{2}}\int_{\mathbf{v}}^{\infty}\mathbf{e}^{-\frac{\mathbf{i}\pi\mathbf{t}^2}{\mathbf{2}}}\mathbf{dt} \quad (5)$$

and approximation ($\mathbf{v} > -0.7$) for diffraction loss in dB:

$$J(v) = 6.9 + 20\log\left(\sqrt{(v-0.1)^2+1} + v - 0.1\right) \quad (6)$$

For detailed maps prediction accuracy of RT, channel modeling is high [15]. The main hardship is complexity, which can be reduced with minimum storage and computation techniques. For these reasons, the following methods were used for the acceleration of tracing in the C++ simulator:

- BVH (Bounding Volume Hierarchy) is a method [16] used for compact storage and reduced intersection testing. To decrease the number of objects to compare, each object and UE are mapped to a spatial grid, so that ray has interfered only with objects in a current grid cell.
- Parallelepiped wrappers are utilized to perform fast initial intersection tests and discard objects without complex surface processing.
- Fast implementation of 3D geometry for ray tracing [17-18] with an extensive application of fast ray-triangle intersection [19].

4. POSITIONING

4.1. Independent AoA Estimation

Firstly, each RRU estimates independently high-resolution angular spectrum from received SRS, e.g., via MUSIC algorithm [20] or smoothing modifications [21].

$$\mathbf{S}(\boldsymbol{\varphi},\boldsymbol{\theta}) = \frac{\mathbf{1}}{\mathbf{a}^{\mathbf{H}}(\boldsymbol{\varphi},\boldsymbol{\theta})\mathbf{V}\mathbf{V}^{\mathbf{H}}\mathbf{a}(\boldsymbol{\varphi},\boldsymbol{\theta})} \quad (7)$$

$$\mathbf{a}(\boldsymbol{\varphi},\boldsymbol{\theta}) = \boldsymbol{\Delta}_{\mathbf{x}}^{i}\cos(\boldsymbol{\theta})\sin(\boldsymbol{\varphi}) + \boldsymbol{\Delta}_{\mathbf{y}}^{i}\cos(\boldsymbol{\theta})\cos(\boldsymbol{\varphi}) + \boldsymbol{\Delta}_{\mathbf{z}}^{i}\sin(\boldsymbol{\theta}) \quad (8)$$

$$\begin{pmatrix}\boldsymbol{\Delta}_{\mathbf{x}}^{\mathbf{i}}\\ \boldsymbol{\Delta}_{\mathbf{y}}^{\mathbf{i}}\\ \boldsymbol{\Delta}_{\mathbf{z}}^{\mathbf{i}}\end{pmatrix} = \begin{pmatrix}(\mathbf{i}_{\mathbf{h}}-\mathbf{1})\mathbf{d}_{\mathbf{h}}\cos(\boldsymbol{\varphi}_{\mathbf{h}}) + (\mathbf{i}_{\mathbf{v}}-\mathbf{1})\mathbf{d}_{\mathbf{v}}\sin(\boldsymbol{\varphi}_{\mathbf{h}})\sin(\boldsymbol{\theta}_{\mathbf{v}})\\ (\mathbf{i}_{\mathbf{h}}-\mathbf{1})\mathbf{d}_{\mathbf{h}}\sin(\boldsymbol{\varphi}_{\mathbf{h}}) - (\mathbf{i}_{\mathbf{v}}-\mathbf{1})\mathbf{d}_{\mathbf{v}}\cos(\boldsymbol{\varphi}_{\mathbf{h}})\sin(\boldsymbol{\theta}_{\mathbf{v}})\\ (\mathbf{i}_{\mathbf{v}}-\mathbf{1})\mathbf{d}_{\mathbf{v}}\cos(\boldsymbol{\theta}_{\mathbf{v}})\end{pmatrix} \quad (9)$$

where V – matrix whose columns are noise eigenvectors, $a(\varphi,\theta)$ – steering vector of antenna panel with $\boldsymbol{\theta}_{\mathbf{v}}$ – tilt and $\boldsymbol{\varphi}_{\mathbf{h}}$ – rotation of antenna array in the horizontal plane. AoAs are estimated from the spectrum $\mathbf{S}(\boldsymbol{\varphi},\boldsymbol{\theta})$ via CA-CFAR (Cell Averaging Constant False Alarm Rate) detector:

$$\mathbf{I}[\{\boldsymbol{\varphi}_{\mathbf{n}},\boldsymbol{\theta}_{\mathbf{n}}\}] = \mathbf{I}\left[P(\varphi_n,\theta_n) > \frac{C_{threshold}}{N_\varphi N_\theta}\sum_{\substack{i=-\frac{N_\varphi}{2}\\ i\neq 0}}^{\frac{N_\varphi}{2}}\sum_{\substack{k=-\frac{N_\theta}{2}\\ k\neq 0}}^{\frac{N_\theta}{2}} P(\varphi_{n-i},\theta_{n-k})\right] \quad (10)$$

4.2. Joint Estimation of Spatial Probability Density

Cloud CU receives noisy estimates of angles $\boldsymbol{\Omega}^{\mathbf{est}} = \{\boldsymbol{\varphi}_{\mathbf{n}},\boldsymbol{\theta}_{\mathbf{n}}\}$ from each DU and searches for the positions by launching rays in close directions $\boldsymbol{\Omega}^{\mathbf{est}} + \boldsymbol{\Omega}^{\mathbf{bias}}$. Intersections of multiple rays from several RRUs define possible emitter locations. Each of positions $\{\mathbf{P}_{\mathbf{x,y,z}}^{\mathbf{i}}\}_{\mathbf{i=1}}^{\mathbf{N_{pos}}}$ is associated with probabilities of received rays and the expectation-maximization leads to:

$$\mathbf{P}_{\mathbf{x,y,z}} = \frac{\mathbf{1}}{\sum_{\mathbf{i}}\mathbf{w}_{\mathbf{i}}}\sum_{\mathbf{i}}\mathbf{w}_{\mathbf{i}}\,\mathbf{P}_{\mathbf{x,y,z}}^{\mathbf{i}} \quad (11)$$

The Bayesian approach can be used to cope with angle estimation errors caused by interference and residual inter-RRU calibration errors:

$$\mathbf{P}(\boldsymbol{\Omega}_{\mathbf{bias}}|\boldsymbol{\Omega}_{\mathbf{est}}) = \frac{\mathbf{P}(\boldsymbol{\Omega}_{\mathbf{est}}|\boldsymbol{\Omega}_{\mathbf{biased}})\mathbf{P}(\boldsymbol{\Omega}_{\mathbf{biased}})}{\mathbf{P}(\boldsymbol{\Omega}_{\mathbf{est}})} \quad \mathbf{(12)}$$

where $\boldsymbol{\Omega}_{\mathbf{est}}$ – biased estimation of angle (azimuth or elevation) received from DU, $\boldsymbol{\Omega}_{\mathbf{bias}}$ – small angle deviation from received direction. $\mathbf{P}(\boldsymbol{\Omega}_{\mathbf{biased}})$ – unique for certain RRU antenna panel and does not depend on UE (e.g., $\mathbf{P}(\boldsymbol{\Omega}_{\mathbf{biased}}) \sim \mathbf{N}(\mathbf{0}, \frac{|\Omega_{\mathbf{biased}}^{max}|}{\mathbf{3}})$), $\mathbf{P}(\boldsymbol{\Omega}_{\mathbf{est}}|\boldsymbol{\Omega}_{\mathbf{biased}})$ – related to estimation from angular spectrum (peak value and peak width) for each found ray.

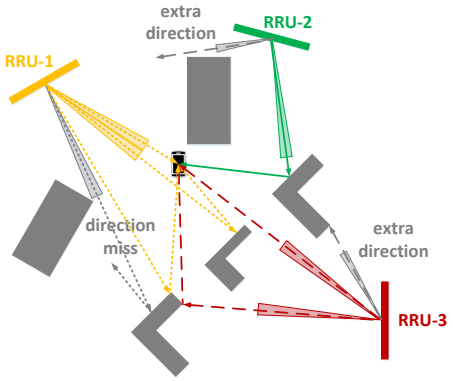

Figure 5. Ray search at CU via RT and known propagation environment.

$$\mathbf{w_i} = \sum_{\mathbf{r=1}}^{\mathbf{N_{rays}}} \mathbf{P}(\boldsymbol{\Omega}_{\mathbf{est}}|\boldsymbol{\Omega}_{\mathbf{biased}})\mathbf{P}(\boldsymbol{\Omega}_{\mathbf{biased}}) \quad \mathbf{(13)}$$

At the end of this step each found position $\mathbf{P}^{\mathbf{i}}_{\mathbf{x,y,z}}$ is described with its probability $\mathbf{w_i}$. From formula (11) we may find a single state maximum expected position. For some cases (e.g., UE has a connection to several RRUs) this estimate will be enough to produce the only dense cluster with a weighted center very close to the real position.

4.3. Optimal Position Selection

At this stage development of algorithms for the joint processing of positions and RT, model outputs have high prospects and research possibilities. RT outputs may include a number of rays, the number of reflections per each ray, the closeness ray to reflecting/diffracting edges, LOS/NLOS recognition, the number of BSs, power level indicators, specific hardware limits of antennas, and others. Processing of the parameters above requires much fewer computing resources than an application of the RT model. At the same time, such an algorithm can enhance the selection of the most probabilistic positions via the recognition of typical patterns. Performance gain can be achieved by taking into account correlations between algorithm positioning errors and physical propagation conditions which are in general related to side RT outputs. As you can see in section 5, even the simplest parameters such as the number of BSs or LOS/NLOS indicators are good predictors of errors.

4.4. Clustering of Probabilistic Estimates of Position

Clustering algorithm

1. Estimate table of distances. Initialize minimum distance between clusters $d_{cluster}$.
2. Perform DF (Depth-First search) of connected subgraphs with condition of connectivity: $d_{i,k} < d_{cluster}$
3. Find clusters' centers from formula (11) and corresponding variances.

In general cases, erroneous angle acquisition may cause tracking extra directions (e.g., in music algorithm it is caused by interference) or direction miss (e.g., small search area). These errors lead to the decomposition of all positions into several remote clusters. Despite the probability of fake clusters is typically low, it slightly decreases the accuracy of estimation. To increase accuracy, we need to perform simple clustering of all positions and exclude fake clusters from consideration.

First step of proposed clustering approach has complexity $\mathbf{O(N_{pos}^2)}$, while the second and third steps are linear. In order to exclude storage of large table (memory ~ $\mathbf{O(N_{pos}^2)}$) of distances this algorithm can be replaced with similar with storage of logical vector of added positions (memory ~ $\mathbf{O(N_{pos})}$).

If the following tracking is not being exploited the most likely cluster is used for selection of optimal position (weighted with probabilities / max posterior position / combining / more sophisticated with RT outputs).

4.5. Tracking in Angular Domain

AoA knowledge is equivalent to knowledge about position for accurate 3D maps. Tracking of direct measurement (angles) is more appropriate than mediated because the error distribution for the first one is more understandable, while the second one may produce biased trajectory. Due to calibration residuals, interference and scattering estimate for azimuth/elevation is close to mixture of uniform and normal/cauchy distributions or contaminated ones. For these reasons L2 optimization is less appropriate for tracking [22] rather then Lp (1<p<2) which is closer to median (L1). Another reason to choose L1 were simulations, resulted in better error reduction mainly due to ability to cope with outliers.

AoA tracking algorithm

Do for each TTI with new AoA estimate:

1. Start trend from new angle estimate.
2. Check whether new estimate can be used to update current trends.
3. Fit each single trend to a new estimate.
4. Check for redundant trends.
5. Erase noisy, redundant and outdated trends, shrink buffers.
6. Predict angles with corresponding trend deviations.

$$\cos(\Omega_{TTI_i} + \Delta\Omega) \approx \cos(\Omega_{TTI_i}) - \sin(\Omega_{TTI_i})\Delta\Omega \quad (14)$$

Figure 6 represents assumptions for the developed AoA tracking system. It includes a linear change of noised AoA between TTI (from steering vectors (9) and long distance to tracking object (14)), AoA estimation miss, false AoA detection, sudden AoA change (UE changed traveling direction or got around the corner of the building) and irregular TTI structure. AoA tracking is done for each antenna array and azimuth/elevation independently. Lp fit for a single trend is described in [23].

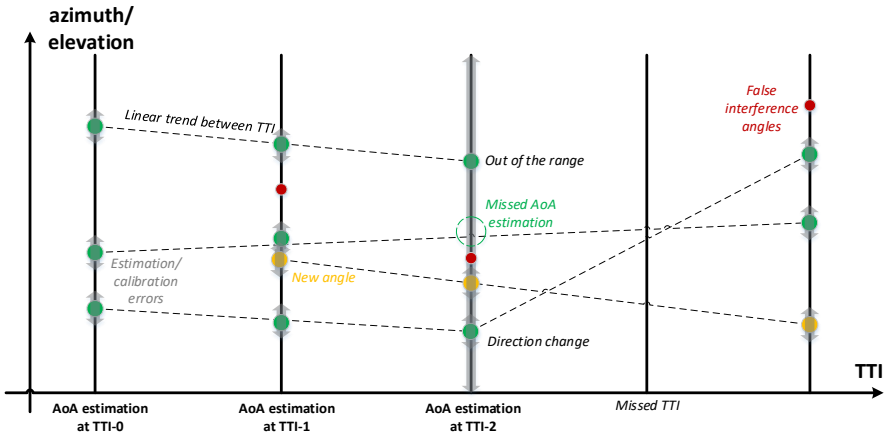

Figure 6. Assumptions for angle tracking model.

Angle predictions are used then for RT positioning with probabilistic weights (13) and additional weights from trend deviations from azimuth and elevation:

$$w_{ray} = \frac{N_{buffer}}{\sum_{i=1}^{N_{buffer}} |\Omega_i - a_{trend} \cdot TTI_i - b_{trend}|^p} \quad (15)$$

The same tracking system without separation for several trends is used for main cluster tracking. Figure 7 reveals the idea for cluster tracking.

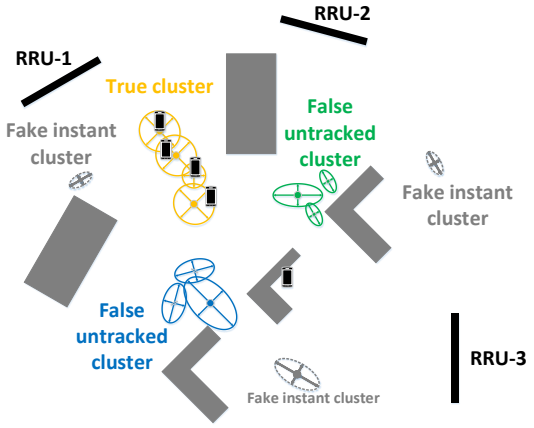

Figure 7. Representation of clusters tracking.

4.6. Accuracy Control

Estimation both of position and predicted error is important for combining RT with other positioning approaches. For RT great errors in instant position estimation can be controlled by comparison with measurements for received power and time differences (not taken into account in this paper). Another way is to exploit RT outputs as described in section 4.3. E.g., miss can be estimated via variance of maximum likelihood points:

$$\mathbf{I}\{\mathbf{P_{x,y,z}} = \mathbf{miss}\} = \mathbf{I}\{\mathbf{D}[\mathbf{P^i_{x,y,z}}] > \boldsymbol{\varepsilon_0}\} \quad \mathbf{(16)}$$

5. SIMULATION RESULTS

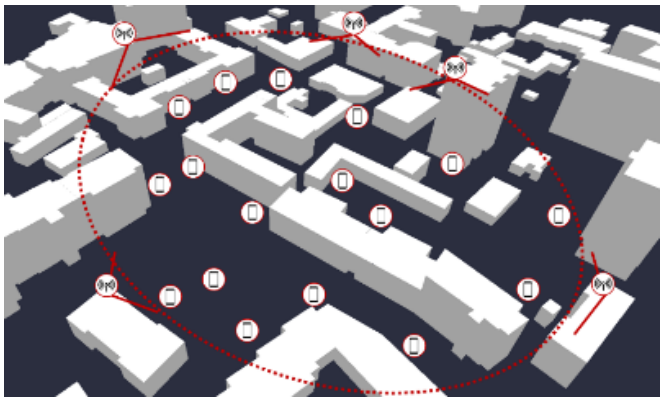

Figure 8. Example of studied Outdoor Environment.

5.1. Positioning Accuracy

Figure 8 represents a simulated Urban Environment, parsed from the OSM map. Base stations' antenna arrays were placed at the top of the buildings. Figure 9 shows how the RT localization principle works:

- base station estimates angular spectrum and detects 3 directions;
- CRAN performs RT approach and detects a position of UE

In the case of accurate localization estimated CIR might be improved. Very close taps (e.g., LOS and ground reflection) might be distinguished. This result might be also used for more accurate beamforming calculations for open-loop systems.

Figure 10 shows CDF of positioning error of single-state position estimation. It is noticeable that impairments that lead to erroneous angle acquisition also cause dramatic decrease of positioning accuracy. Second graph demonstrates that low accuracy of phase calibration of antenna panel for NLOS cases makes RT positioning without clustering and position selection not robust.

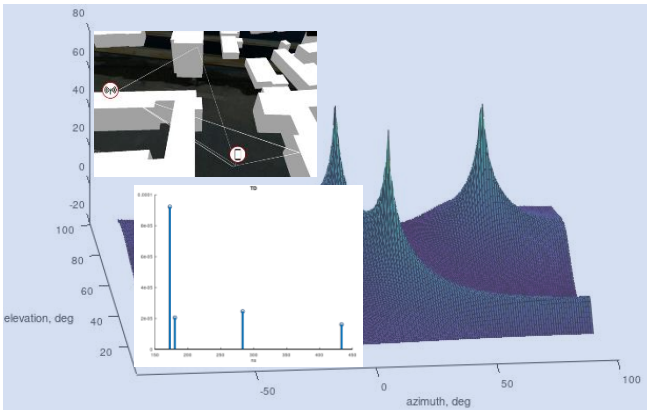

Figure 9. Example of high precision angular spectrum estimation and ray tracing for positioning and CIR reconstruction.

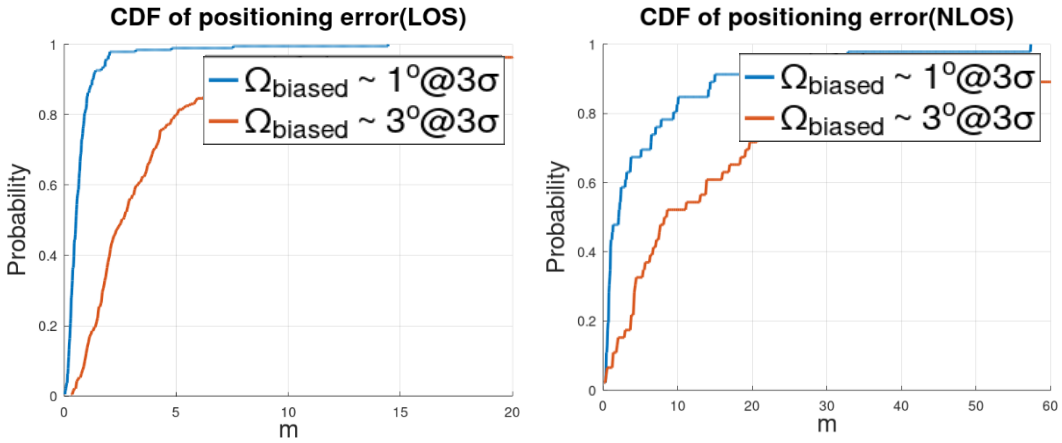

Figure 10. CDF of error of joint estimation of the most likely position (after step 4.2).

Table 1 demonstrates dependence of positioning error on the number of base stations used for SRS acquisition. The high positioning error occur primarily due to the points of poor radio coverage, where the use of several base stations is limited. If we take into account that such points are known in advance, then it is possible to control this error. Research has shown that such areas are related to reception of signal from single collocated antenna array with very low SNR and sparse NLOS channel.

Table 1. Localization accuracy with dedicated maximum number of base stations.

LOS&NLOS +/- 1^0@3σ, without tracking					
Nbs	1	2	3	4	5
90% percentile for absolute error	15m	2m	1.6m	1.3m	1m

Figure 11 represents CDF of positioning error (+/- 2^0) with clustering and rejection of position candidates by the only flexible threshold for number of rays. Previously it was mentioned that impairments can cause fake remote position candidates to appear and decrease accuracy significantly. Such misdetection was solved with selection of the most likely cluster (e.g., in figure 12). Inside cluster several approaches can be used:

- Position with maximum posterior probability
- Most expected position, averaged in cluster

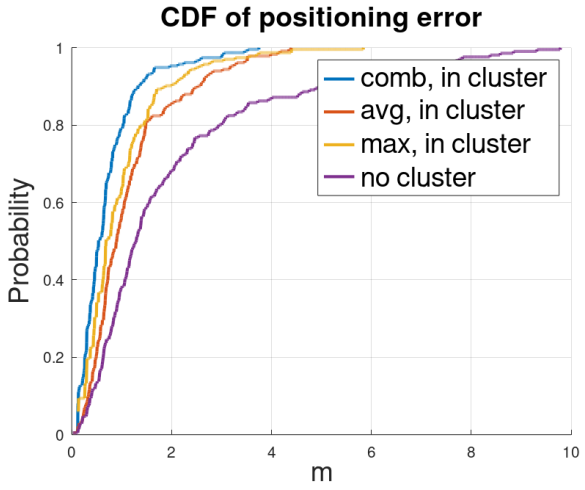

Figure 11. CDF of error of joint estimation of expected position with main cluster selection (after step 4.4).

Both of these strategies are presented in graph as well as their combination. Optimal clustering provides positioning error with Pr = 0.9 less than 1.3m for typical mixed LOS/NLOS Urban Outdoor scenario while without clustering 1.3m is reached with Pr = 0.5. In case of more accurate phase synchronization (+/- 1^0@3σ) at the same probability level localization accuracy reaches 0.9m, which perfectly fits 5G NR requirements for accuracy [24-25].

True positioning error is highly correlated to interim assessment of position variance among a set of possible positions with Pearson correlation coefficient = 0.7, which means that the most of predicted positions can be estimated with very close errors. Better error control as mentioned earlier can be achieved by matching positions with exact patterns from RT outputs.

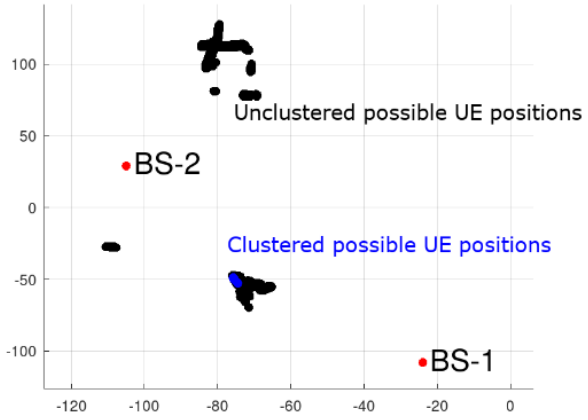

Figure 12. Example of clustering of candidates for UE position

Figures 13-14 represent example of UE trajectory in NLOS and corresponding tracking error. Highest errors (above 1m) happen during direction change in sparse NLOS conditions. After UE enters LOS area (after 310 TTI, TTI = 10 frames) tracking adapts much faster and error mostly does not exceed 1m after convergence.

Figure 13. Example of UE trajectory.

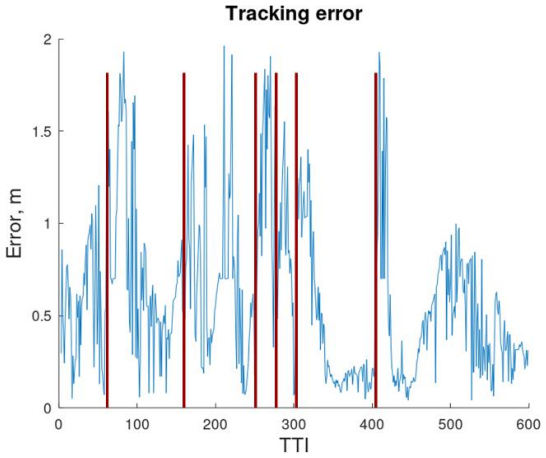

Figure 14. Absolute tracking error across the track (Figure 13). Vertical lines correspond to the moments when UE turns in another direction.

Figure 15 shows UE trajectory in azimuth/time plane from single base station. Predicted (green) have low level of outliers. Such approach can also be useful for management of frequent UE tracks to enhance positioning via storage of previous measurements and use them to predict optimal multiuser beamforming.

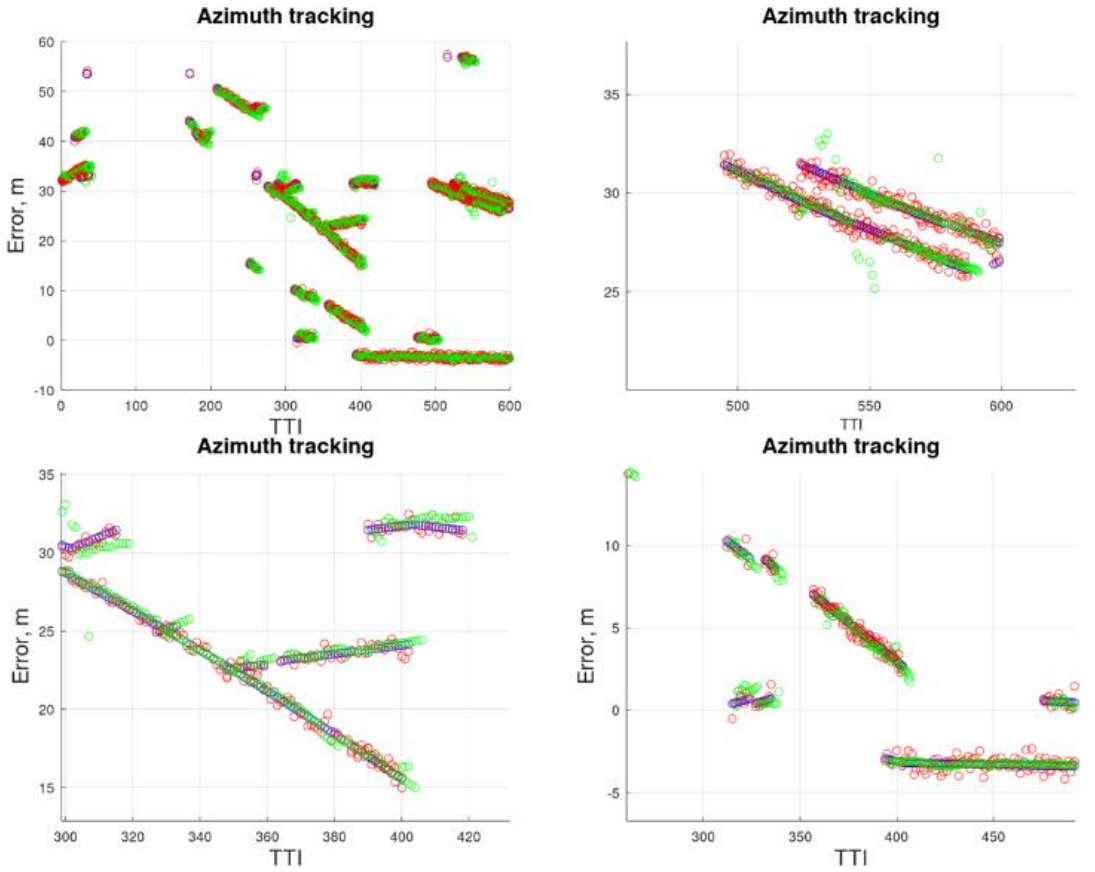

Figure 15. Azimuth tracking of UE trajectory. Blue – true AoA, red – measurement (interference not shown), green – predicted.

5.2. Calibration of Inaccurate Maps

Initially, the most concerns about positioning accuracy were related to the accuracy of the digital map. They were resolved with RT positioning in the map, in which properties of materials (reflection coefficients, scattering model), buildings sizes, and positions are pre-set with errors. Results are summarized in Table 2. These results are very close to the estimate by Monte Carlo method if simulated with known average number of reflections and rays to each UE in 2D space.
As it is shown below inaccurate maps are one of the key factors for decrease of accuracy. Inaccurate maps can be calibrated either online or offline. The first can be solved using GAN models while the second exploits RTK receivers. Here online converging algorithm is presented for calibration of maps based on multiple AoA measurements. At the first stage multiple outputs from RT positioning procedure are collected: AoA estimates, final positions and corresponding directions. Secondly, random object for calibration was selected with all UEs that were affected by the rays from this object. Then multiple of new states of this objects are created (new position, material properties, size, etc.). Finally, me measure mean internal variance of probabilistic estimates of UE positions across selected UEs and calculate gradients of update as differences between new and stored variances. To avoid saturation all UEs corresponding to the object we divided into several groups. Figure 16 shows general idea of object update with decrease of variance of position candidates.

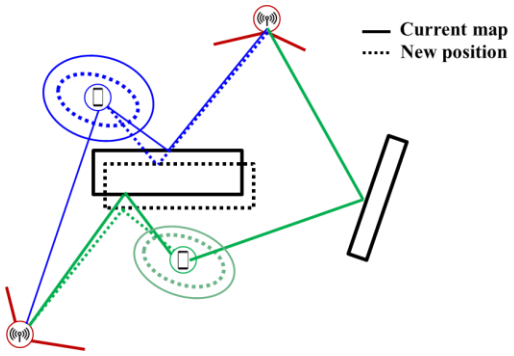

Figure 16. Representation of ray tracing for a new object state.

Table 2 represents decrease of positioning error in inaccurate map with proposed calibration procedure. Generally, it allows to decrease additional error with relatively small residual one. It was noticed that in cases with poor distribution of UEs in space or its small amount corresponding object was overfitted, which influenced map, but not positioning accuracy. Also, final variances of estimates after calibration were much better correlated with true positioning error (Pearson correlation is up to 0.9).

Table 2. Contribution of map inaccuracy to localization error and map calibration procedure.

	Deviation from true value	**Map without calibration**		**Calibrated map**
		median	**90% percentile**	**90% percentile**
	no	0.7 m	1.3 m	1.3 m
Transmission coefficient	$Uniform(50\%, 200\%)$	1 m	1.7 m	1.5 m
	$Uniform(80\%, 150\%)$	0.8 m	1.5 m	1.4 m
Building, walls position	$N(0\ m, 1\ m)$	1.2 m	2.1 m	1.5 m
	$N(0\ m, 2\ m)$	1.5 m	2.5 m	1.5 m

The most of increase of position error from inaccurate map came from UE with a little number of rays or served by the only base station. Also ray search area has to be increased to partly mitigate error.

5.3. Comparison of Measurements and Simulations

Simulation results above were compared [26] with real GPS measurements in the same outdoor positions as simulated. About 1000 measurements were done both via Samsung Galaxy Note 8 (*GPS Test* software) and iPhone SE (*GPS Data Smart* software). The following metrics were collected for each measurement:

- Horizontal accuracy

Internal software estimate of positioning accuracy corresponding to 68% confidence interval.

- Measured accuracy

Absolute difference of positions in Google or Yandex maps and real environment (compared to surrounding buildings)

Table 3 provides results of experiment and compares with simulations (with combined cluster selection, but without tracking). On average proposed approach has a several times higher accuracy than GNSS one.

Table 3. Comparison between accuracy of measurements and simulations.

		median	90% percentile
Note 8	Horizontal accuracy	5.2 m	8.9 m
	Measured accuracy	4.7 m	8.6 m
iPhone SE	Horizontal accuracy	5.0 m	7.9 m
	Measured accuracy	7.6 m	11..2 m
Simulated	1^0@3σ	0.5 m	1.2 m
	3^0@3σ	0.7 m	1.5 m

Figure 17. Example of usage GPS Test and Yandex Maps for single measurement.

6. APPLICATION OF RT FOR CHANNEL PREDICTION

One of possible applications of Ray Tracing model apart from pure positioning is precoder/channel tracking. Predicted position of UE can be used for beamforming calculation. Article [27] contains generalized MU precoder design, which was used for sum rate calculation. UEs channel matrices are merged together:

$$H^{ue} = \left[H_1 \dots H_{ue-1} H_{ue+1} \dots H_{N_{ue}}\right]^T,\ H_{ue} \to [N_{rx} * (N_{bs} * N_{tx})]$$

to find orthogonal projection:

$$H^{ue} = USV^H,\ W = V\left(SS^H + \frac{\sigma^2}{P_{BS}} I\right)^{-\frac{1}{2}}.$$

UE channel matrix is projected into it:

$$H_{ue} W = USV^H.$$

And the final precoder is:

$$P_{ue} = W * V.$$

Under the assumption of full-digital of hybrid [28-29] beamforming predicted position of UE was converted to CIR and was used for beamforming calculation. Figure 18 represents trajectory of

two pedestrians which were scheduled for simultaneous DL transmission. UE is equipped with single antenna; BS is equipped with 8 antennas. MU precoder is calculated once at the start of two trajectories.

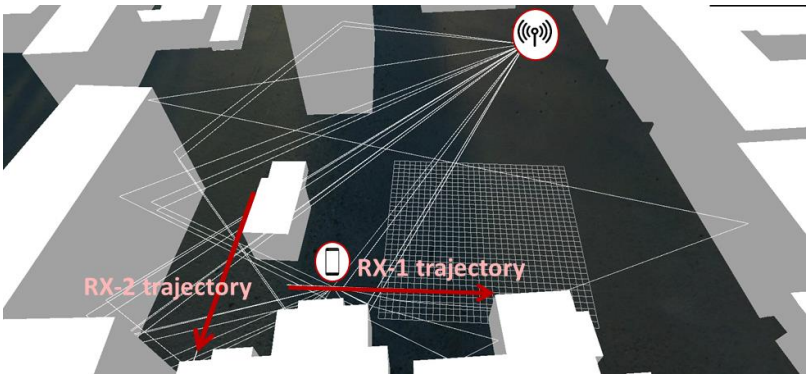

Figure 18. Forward trajectory of two pedestrian UE.

Figure 19 compares sum rate along UE track with two precoding strategies: MU and SU. 'Old' suffix corresponds to the precoder calculated once in the beginning of track, 'instant' corresponds to the precoding with ideal knowledge of channel. As it can be seen from this example channel aging results that MU precoder performs worse or almost the same as SU one, while possible gain in from RT predicted channel in this case is 2x capacity.

Table 4 represents capacity gain achieved with proposed RT tracking for MU and SU precoding. MU precoder is calculated for UE pairs, matched by channel orthogonality. Reference precoder is calculated once in 10 sec. Simulation conditions are the same as above.

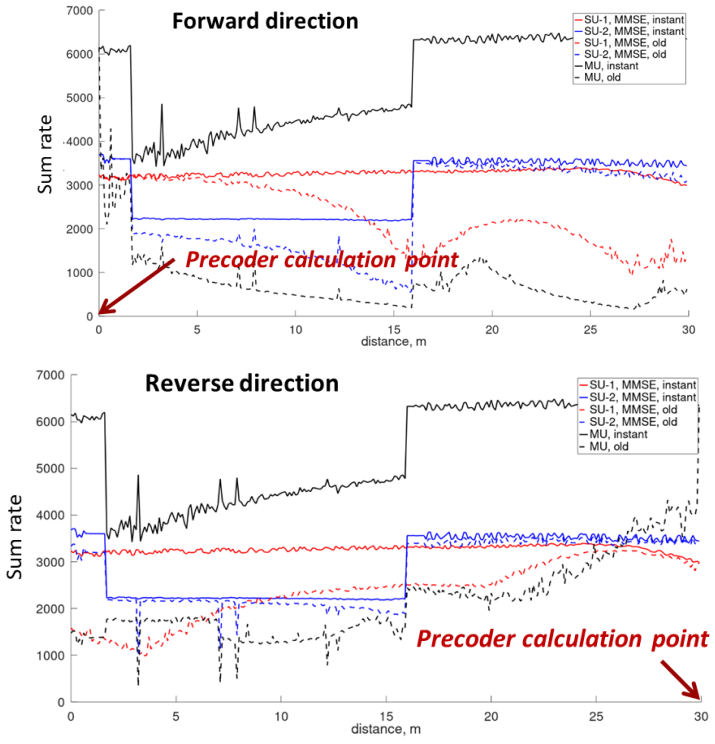

Figure 19. Sum rate comparison for several precoding strategies.

Prediction of SU precoder in NLOS gives up to 30%, which is good result, but under practical implementation does not seem so desirable. Despite SU precoder in LOS shows better results than in NLOS, tracking in this case might be much less complex than with RT. The most sum rate gain corresponds to MU precoding. Reduction of allocated resources for channel sounding was not taken into account here. Thus, MU precoder calculation in advance with RT predictions seems the most promising application.

Table 4. Average approximate simulated sum rate gain from utilization of RT tracking.

AoA accuracy		$1^0@3\sigma$	$2^0@3\sigma$
SU, LOS	MMSE	40%	35%
	ZF	60%	40%
SU, NLOS	MMSE	15%	15%
	ZF	30%	25%
MU	---	80%	60%

Apart from TDD channel prediction RT approach may improve theoretical lower bound of FDD channel extrapolation [30] and reduce receiver complexity.

7. ANTENNA CALIBRATION

In order to achieve high accuracy of the angular spectrum estimation, precise installation of base station antennas is required as well as stricter requirements for wind load and accuracy of positions of base stations. These issues require to remove bias from estimated AoA and location of UE by correction with averaged by UE estimates of obtained via RT weighted rays and positions. This correction values are calculated at CPU and reported to DU.

One of the main advantages of proposed positioning approach is that network time synchronization between different units is enough as well as no extra requirements for frequency synchronization needed. At the same time each 10 ns delays difference in tx/rx chains adds 4.2 meters error for 1 BS and 2.4 for 3 BSs with TDOA positioning, which is much higher than with proposed approach. But according to [31] time alignment error might be up to 65 ns between antenna ports, which makes impossible accurate AoA estimation and requires calibration procedure.

Typical 8T8R antenna includes additional calibration port [32] to remove phase and amplitude differences between RF signals. Self-calibration with embedded transmission lines accuracy is about 6 degrees [33], which is much lower than required to overcome GPS accuracy. Over-the-Air calibration [34-35] provides desired phase accuracy [36] with group-based methods.

8. RT IMPLEMENTATION

The Proposed RT approach for positioning is beneficial for future RAN at least because it produces new independent estimates for joint filters exploiting GPS, sensors, TDoA from base stations, etc. It transfers the main load to the server and does not burden edges with large computations and has minimum backhaul traffic.

Another important issue to mention is the fast, low-complex, and memory-efficient RT model. For the only purpose of positioning, it can be effectively stored in a database containing sets

<angle, position, RT outputs> where RT outputs links to another database <index, object description>. RT outputs are any important parameters that can enhance the optimal position selection stage or be used for other prediction needs. Many simulated cases have shown that via C++ from several seconds to several days (depending on accuracy, details, map size) may be required to simulate with a single thread. These seems to be opportunistic, because it should be done once to fill the database of several Gb. Also due to rays are independently propagate these computations can be easily parallelized and also some parts of database could be upgraded if propagation environment has changed without complete computation.

When required database is ready for the use the most complexity is related to accurate AoA estimation. Calculation of spatial probability density is done in parallel as well as selection of position candidates. Clustering complexity is closely related to the latter. As a rule, all this requires 10-1000 times fewer basic operations.

9. CONCLUSIONS

This paper covered the RT positioning technique for the Urban Outdoor scenario and supplemented previously studied positioning algorithms. It was shown that impairments and interference cause pure RT positioning to fail in NLOS. Developed clustering approach of probabilistic candidates for positions mostly mitigated this error and provided almost the same accuracy as for LOS case. The Proposed positioning framework was compared to measurements and demonstrated much better accuracy. For 90% of Outdoor cases RT positioning may provide ~0.9-2.5m accuracy, which is enough for most 5G use cases.

Also, the proposed 3D map calibration procedure has shown significant performance gain in low-precision maps. Additional error ~1m from inaccurate maps was mostly mitigated with it.

Developed low complex tracking system in angular domain demonstrated ability to efficiently cope with angle acquisition outliers. As simulated with fully digital precoder such tracking for channel prediction improves capacity at least for several dozens of percent and up to 80% for multiuser.

RT positioning has a good internal assessment of error, which enables to combine it with other positioning systems. Also, it enables realistic scheduling, improved resource allocation, channel prediction and extrapolation.

FUTURE RESEARCH

In the future, it is expected to develop a prediction model for a low-complex probabilistic SU/MU-MIMO hybrid precoder with the use of RT and angle tracking. Another important issue is related to the development and implementation of distributed calibration procedures.

CONFLICTS OF INTERESTS

The author declares no conflict of interest.

ACKNOWLEDGEMENTS

This paper will not be possible without the support of Anton Laktyushkin. His knowledge and critics let me avoid many common mistakes in this work. I would also like to thank all the colleagues from Huawei Moscow Research Center with whom I had the opportunity to work.

REFERENCES

[1] Sand, S.; Dammann, A.; Mensing, C. Positioning in Wireless Communication Systems; John Wiley & Sons Ltd.: Hoboken, NJ, USA, 2014.

[2] C. Shepard, H. Yu, N. Anand, E. Li, T. Marzetta, R. Yang, and L. Zhong, "Argos: Practical Many-antenna Base Stations," in Proc. of the 18th Annual Intl. Conf. on Mobile Computing and Networking, Aug. 2012, pp. 53–64.

[3] K. Li, R. R. Sharan, Y. Chen, T. Goldstein, J. R. Cavallaro and C. Studer, "Decentralized Baseband Processing for Massive MU-MIMO Systems," in IEEE Journal on Emerging and Selected Topics in Circuits and Systems, vol. 7, no. 4, pp. 491-507, Dec. 2017, doi: 10.1109/JETCAS.2017.2775151.

[4] Y. Wang, Z. Shi, Y. Yu, S. Huang and L. Chen, "Enabling Angle-based Positioning to 3GPP NR Systems," 2019 16th Workshop on Positioning, Navigation and Communications (WPNC), 2019, pp. 1-7, doi: 10.1109/WPNC47567.2019.8970182.

[5] Marsch, P., & Fettweis, G. (Eds.). Coordinated Multi-Point in Mobile Communications: From Theory to Practice. 2011. Cambridge: Cambridge University Press. doi:10.1017/CBO9780511783029

[6] Vladislav Ryzhov, "Robust Outdoor Positioning via Ray Tracing," Computer Science & Information Technology pp. 149-164, https://doi.org/10.5121/csit.2023.130513.

[7] 3GPP, TR 138 901, Release 14, Study on channel model for frequencies from 0.5 to 100 GHz, 2017-05

[8] 3GPP, TS 38.211, Release 15, Physical channels and modulation, 2018-07

[9] A. W. Mbugua, Y. Chen, L. Raschkowski, L. Thiele, S. Jaeckel and W. Fan, "Review on Ray Tracing Channel Simulation Accuracy in Sub-6 GHz Outdoor Deployment Scenarios," in IEEE Open Journal of Antennas and Propagation, vol. 2, pp. 22-37, 2021, doi: 10.1109/OJAP.2020.3041953.

[10] Kong, Fanzeng et al. "A GDOP-Weighted Intersection Method for Ray-Trace Based Target Localization using AOA Measurements in Quasi-Specular Environment." (2016).

[11] del Corte Valiente, Antonio & Gómez, José & Gutiérrez-Blanco, Oscar & Castillo-Sequera, Jose. (2019). Localization Approach Based on Ray-Tracing Simulations and Fingerprinting Techniques for Indoor–Outdoor Scenarios. Energies. 12. 2943. 10.3390/en12152943.

[12] Tayebi, Abdelhamid et al. "The Application of ray-tracing to mobile localization using the direction of arrival and received signal strength in multipath indoor environments." Progress in Electromagnetics Research-pier 91 (2009): 1-15.

[13] V. Degli-Esposti, F. Fuschini, E. M. Vitucci and G. Falciasecca, "Measurement and Modelling of Scattering From Buildings," in IEEE Transactions on Antennas and Propagation, vol. 55, no. 1, pp. 143-153, Jan. 2007, doi: 10.1109/TAP.2006.888422.

[14] Recommendation ITU-R P.526.11, Propagation by diffraction, The international telecommunication union, 10/2009.

[15] T. Fugen, J. Maurer, T. Kayser and W. Wiesbeck, "Verification of 3D Ray-tracing with Non-Directional and Directional Measurements in Urban Macrocellular Environments," 2006 IEEE 63rd Vehicular Technology Conference, 2006, pp. 2661-2665, doi: 10.1109/VETECS.2006.1683351.

[16] Fabianowski, Bartosz & Dingliana, John. (2009). Compact BVH Storage for Ray Tracing and Photon Mapping.

[17] Andrew S. Glassner, James Arvo, David Kirk. Graphics Gems, I, II, III, Academic Press, 1990-1992.

[18] Daniel Sunday. Practical Geometry Algorithms: with C++ Code, 2021

[19] Möller, Tomas & Trumbore, Ben. (2005). Fast, Minimum Storage Ray-Triangle Intersection. Journal of Graphics Tools. 2. 10.1145/1198555.1198746.

[20] R. Schmidt, "Multiple emitter location and signal parameter estimation," in IEEE Transactions on Antennas and Propagation, vol. 34, no. 3, pp. 276-280, March 1986, doi: 10.1109/TAP.1986.1143830.

[21] V. Molodtsov, A. Kureev and E. Khorov, "Experimental Study of Smoothing Modifications of the MUSIC Algorithm for Direction of Arrival Estimation in Indoor Environments," in IEEE Access, vol. 9, pp. 153767-153774, 2021, doi: 10.1109/ACCESS.2021.3127861.

[22] Narula, S.C. (1987). The Minimum Sum of Absolute Errors Regression. Journal of Quality Technology, 19, 37-45.

[23] Sposito, V.A., Kennedy, W.J., & Gentle, J.E. (1977). Algorithm AS 110: L p Norm Fit of a Straight Line. Applied statistics, 26, 114-118.
[24] Service requirements for the 5G system, 3GPP TS 122 261 - V16.14.0
[25] Study on NR positioning support, 3GPP TR 38.855 V1600
[26] Yan, W., Zhang, Q., Zhang, Y., Wang, A., Zhao, C. (2021). The Validation and Performance Assessment of the Android Smartphone Based GNSS/INS Coupled Navigation System. In: Yang, C., Xie, J. (eds) China Satellite Navigation Conference (CSNC 2021) Proceedings. Lecture Notes in Electrical Engineering, vol 772. Springer, Singapore. https://doi.org/10.1007/978-981-16-3138-2_30
[27] Stankovic, Veljko; Haardt, Martin (2008). Generalized Design of Multi-User MIMO Precoding Matrices. IEEE Transactions on Wireless Communications, 7(3), 953–961. doi:10.1109/LCOMM.2008.060709
[28] X. Yu, J. -C. Shen, J. Zhang and K. B. Letaief, "Alternating Minimization Algorithms for Hybrid Precoding in Millimeter Wave MIMO Systems," in IEEE Journal of Selected Topics in Signal Processing, vol. 10, no. 3, pp. 485-500, April 2016, doi: 10.1109/JSTSP.2016.2523903.
[29] Z. Wang, M. Li, Q. Liu and A. L. Swindlehurst, "Hybrid Precoder and Combiner Design With Low-Resolution Phase Shifters in mmWave MIMO Systems," in IEEE Journal of Selected Topics in Signal Processing, vol. 12, no. 2, pp. 256-269, May 2018, doi: 10.1109/JSTSP.2018.2819129.
[30] F. Rottenberg, R. Wang, J. Zhang and A. F. Molisch, "Channel Extrapolation in FDD Massive MIMO: Theoretical Analysis and Numerical Validation," 2019 IEEE Global Communications Conference (GLOBECOM), Waikoloa, HI, USA, 2019, pp. 1-7, doi: 10.1109/GLOBECOM38437.2019.9013411.
[31] 3GPP TS 38.104 version 17.5.0 Release 17
[32] 8T8R Antenna Beamforming Technology Introduction, Huawei WP
[33] C. Guo, L. Tian, Z. H. Jiang and W. Hong, "A Self-Calibration Method for 5G Full-Digital TDD Beamforming Systems Using an Embedded Transmission Line," in IEEE Transactions on Antennas and Propagation, vol. 69, no. 5, pp. 2648-2659, May 2021, doi: 10.1109/TAP.2020.3030980.
[34] M. Jokinen, O. Kursu, N. Tervo, J. Saloranta, M. E. Leinonen and A. Pärssinen, "Over-the-Air Phase Measurement and Calibration Method for 5G mmW Phased Array Radio Transceiver," 2019 93rd ARFTG Microwave Measurement Conference (ARFTG), Boston, MA, USA, 2019, pp. 1-4, doi: 10.1109/ARFTG.2019.8739190.
[35] D. Glamocic and S. Tomasin, "Calibration of mmWave Antenna Arrays for Initial Access in Massive MIMO 5G Cellular Networks," 2019 IEEE 20th International Workshop on Signal Processing Advances in Wireless Communications (SPAWC), Cannes, France, 2019, pp. 1-5, doi: 10.1109/SPAWC.2019.8815507.
[36] Cao, Yang & Wang, Pan & Zheng, Kang & Liang, Xianghu & Liu, Dongjie & Lou, Mengting & Jin, Jing & Wang, Qixing & Wang, Dongming & Huang, Yongming & Xiaohu, You & Wang, Jiangzhou. (2022). Experimental Performance Evaluation of Cell-free Massive MIMO Systems Using COTS RRU with OTA Reciprocity Calibration and Phase Synchronization.

AUTHORS

Vladislav Ryzhov is a researcher and developer in the field of LTE/5G. He received B.S. degree in MIPT in the field of applied mathematics and physics in 2021 and continued his studies towards M.S. He has an industry experience in Huawei Technologies Co. Ltd. and Yadro.